



Electrically conductive polymer composite containing hybrid graphene nanoplatelets and carbon nanotubes: synergistic effect and tunable conductivity anisotropy

Xiaoling Luo¹ · Guanda Yang^{1,2} · Dirk W. Schubert^{1,2}

Received: 15 June 2021 / Revised: 19 July 2021 / Accepted: 6 August 2021 / Published online: 30 September 2021
© The Author(s) 2021

Abstract

Pristine carbon nanotubes (CNTs) and functionalized carbon nanotubes (f-CNTs) were introduced into conductive poly(methyl methacrylate)/graphene nanoplatelet (PMMA/GNP) composites to achieve a synergistic effect in the enhancement of the conductivity and the reduction in the percolation threshold by forming a 3-Dimensional(3-D) hybrid structure. Both the in-plane and perpendicular electrical properties were investigated. The synergies of hybrid fillers in the in-plane direction were more dependent on the total filler loading, while those in the perpendicular direction were significantly influenced by the GNP/CNT or GNP/f-CNT ratios. Typically, a schematic diagram of the evolution of the 3-D conductive pathways of PMMA/GNP/f-CNT composite at different GNP/f-CNT ratios was presented to explain this phenomenon. Moreover, tunable conductivity anisotropy (defined as the ratio of in-plane conductivity to perpendicular conductivity) ranging from 0.01 to 1000 was achieved, simply by constructing different conductive structures at various filler loadings or ratios in composites.

Keywords Conductive polymer composite · Graphene nanoplatelets · Carbon nanotubes · Synergistic effect · Anisotropy

1 Introduction

Conductive polymer composites (CPCs) can be obtained by loading conductive fillers into insulating polymer matrices, which have received intensive attention from both the academy and industry [1]. Among the conductive fillers, carbon nanotubes (CNTs) [2–5] and graphene derivatives like graphene nanoplatelets (GNPs) [6–9] are of particular favor on account of the unique structures and remarkable conductivities. However, due to the relatively high cost of nanoparticles, poor processability, and poor mechanical properties at high filler content, it requires reducing filler concentration as much as possible. Thus much attention is focused on the possibility of achieving a synergistic effect from the presence of two carbon fillers with different geometries and

electrical properties [10, 11]. Excellent material properties and similar molecular structures make CNTs and GNPs the most studied combinations of carbon nanofiller in polymer composites. GNPs have a high specific surface area, unless well separated from each other; GNPs tend to form irreversible agglomerates or even re-stack through van der Waals interactions [12, 13]. When CNTs are introduced, they can both embed graphene nanofillers and bridge the independent graphene layers into an interconnected entire structure [14, 15]. Thus the synergistic effect could occur through the non-covalent π - π interaction, disintegrating agglomerates, and establishing efficient 3-D interconnected conduction paths.

One can define “synergy” in several different ways; the current reported synergy mainly includes the following [16, 17]. (1) A small amount of a second filler dramatically increases the conductivity of the CPC [18–21]. (2) The conductivity of the ternary CPC is higher than the conductivity of either of the two binary CPCs while keeping the total filler fraction constant [22]. (3) The conductivity of the ternary CPC is higher than the conductivities of the both binary CPCs at the same total filler fraction [23–26]. (4) The experimental percolation threshold of the ternary CPC is lower than the predicted connecting line between the

✉ Xiaoling Luo
xiaoling.luo@fau.de

¹ Institute of Polymer Materials, Friedrich-Alexander-University Erlangen-Nuremberg, Martensstr. 7, Erlangen 91058, Germany

² KeyLab Advanced Fiber Technology, Bavarian Polymer Institute, Dr. Mack- Strasse 77, Fürth 90762, Germany

percolation thresholds of the two fillers A and B as given by Eq. 1 [18, 24]:

$$\frac{\Phi_A}{\Phi_{c,A}} + \frac{\Phi_B}{\Phi_{c,B}} = 1 \quad (1)$$

where Φ_A and Φ_B are the actual volume fractions of A and B particles. $\Phi_{c,A}$ and $\Phi_{c,B}$ are the percolation volume fraction of A and B if the unit volume is filled with A or B alone. For polymer/GNPs/CNTs, A and B represent GNPs and CNTs.

Type 1 and 3 synergies were realized in TPU composite [18]; the percolation threshold of GNPs was about 0.006 vol. % when the CNT content was fixed at 0.255 vol. % that is below the percolation threshold of CNTs/TPU nanocomposites. In another research [24], Φ_c was about 0.84 wt% and 0.88 wt% for the composite filled with single CNTs and GNPs, respectively, while that was 0.62 wt% of the hybrid filler system, together with a significant increase in conductivity in the lower overall filler concentration at the ratio of CNTs/GNPs = 8/2, achieving both type 3 and 4 synergies. Such a dependence of the synergistic effect on the filler ratio was usually found in many studies [27–31], which means synergy sometimes only occurs at certain ratios of hybrid fillers and may vary from these ratios. From these studies, one could find that the optimal filler ratio varied from system to system. It is generally believed that the synergy does not always work since the dispersion state of fillers varies, which depends on the ratio of filler loading, interaction between fillers and polymer matrix, and filler size. No synergy or even anti-synergistic effect has been found in some researches. For example, hybrid CNTs/GNP nanocomposites exhibit electrical conductivities similar to single CNT-based nanocomposites [32] or GNP-based nanocomposites [33], while the other filler does not contribute to enhancing the electrical conductivity. However, there is still a lack of systematic analysis of when the synergistic effect appears and fades away and how it changes with the dispersion state of fillers.

It has been reported that the conductivities in different measuring directions can be different, which often results from the orientation of conductive fillers [34–39]. Studies including perpendicular (through-thickness) electrical conductivity mainly focus on the following few categories: (1) Methods of enhancing perpendicular conductivity of carbon fiber reinforced polymer composites to minimize their damage from lightning strikes [40–42]. (2) Methods of inducing filler alignment to improve the electrical properties along the aligning direction [43–46]. (3) Comparison of the effect of different processing-related factors in the orientation state of conductive particles [47, 48]. If efficient 3-D conductive networks form by GNPs/CNTs hybrid in ternary CPCs, conductivities in the in-plane and perpendicular direction must change relative to the binary CPCs. The investigation is of

much interest; however, few studies have been conducted on that. Furthermore, compared to inducing filler alignment with external fields, hybridizing fillers might be a promising and facile way to tune the anisotropic electrical properties.

In this work, pristine CNTs and oxygen functionalized CNTs were added into PMMA together with GNPs to form the ternary composites at different filler ratios. This work aims to study how the structures and morphologies of ternary polymer composites determine the in-plane and perpendicular electrical conductivities systematically. Based on the different 3-D conductive structures at various filler loadings and ratios, a facile route to tune the conductivity anisotropy via hybrid fillers is proposed.

2 Experimental section

2.1 Materials

The matrix material PMMA Plexiglas 7 N was provided by Evonik Röhm GmbH (Germany), with Mw of 99 kg/mol and polydispersity index of 1.52. Tetrahydrofuran (THF) was obtained from Sigma Aldrich, Saint Louis, MO, USA. Nitric acid (70 v/v%) and sulfuric acid (98 v/v%) were provided by Carl Roth GmbH (Germany) and Merck KGaA (Germany), respectively. GNPs were supplied by ProGraphite GmbH (Germany) with about 10 layers, d50 as an index of 50 μm , and conductivity of 800–1100 $\text{S}\cdot\text{cm}^{-1}$. CNTs Baytubes® C150P were obtained from Bayer Material Science AG, Leverkusen, Germany, which has been characterized by a carbon purity of about 95%, and a bulk density of 120–170 kg/m^3 . The length is larger than 1 μm , and an outer nanotube diameter is 13 ± 3 nm according to the datasheet.

2.2 Oxygen functionalization of CNTs

Functionalized CNTs (f-CNTs) were prepared by reacting pristine CNTs with sulfuric and nitric acids. In the reaction, 0.5 g of CNTs powder was added to 40 ml of nitric acid: sulfuric acid (1:3) mixture. After reacting for 24 h, the precipitated powder was carefully removed and washed with distilled water until the pH was neutral [49]. The resultant powder was dried in an oven for 24 h at 80 °C.

2.3 Sample preparations

All materials were dried at 80 °C in a vacuum oven for at least 12 h before processing. GNPs and CNTs (or f-CNTs) of various loadings and ratios were sonicated in THF for 30 min to yield a homogeneous dispersion, and then, PMMA pellets were added into the GNP/CNT/THF or GNP/f-CNT/THF suspensions. The concentration of the polymer solution was kept at about 4 wt% in this work. Next, the obtained

mixtures above were stirred for 24 h at room temperature. Finally, these mixtures were cast onto glass plates and dried under ambient conditions for 48 h. The resultant composite films had a thickness of about 0.2 mm.

2.4 Characterization

Investigation of the qualitative composition of the functional groups on the surface of CNTs and f-CNTs was performed with Fourier transform infrared (FTIR). The spectra were recorded using a Nicolet 6700 spectrophotometer in the frequency range of 4000–500 cm^{-1} in transmission mode (KBr). The macro-scale dispersion of fillers in the PMMA matrix were observed with an optical microscope (OM) (Leitz, Orthoplan P). Scanning electron microscopy (SEM) (Carl Zeiss Microscopy, Germany) was conducted to investigate the morphologies of fillers and composite films, operating at an accelerating voltage of 3 kV. The composite films were previously fractured at room temperature, and the cross-sections were coated with a gold layer using Sputter Coater S150B from Edwards. The electrical resistance R of composites both in the in-plane direction and through-plane direction were measured at room temperature, using a Keithley 6487 Pico ammeter at a constant voltage (1 V) based on a homemade setup as shown in Fig. S1. The electrical conductivity σ was then calculated as

$$\sigma = d/(R \times S) \quad (2)$$

where R is the electrical resistance of the sample, d is the length of the sample parallel to the direction of the voltage or the distance between two electrodes, and S is the area of the sample perpendicular to the direction of the electrical field. Tensile testing was evaluated on a universal test machine (Zwick Z050) with a tensile speed of 1 mm/min. Five samples were tested for each group for both electrical and mechanical tests in order to have an average.

3 Results and discussion

3.1 Structure characterization of carbon fillers and binary composite films

The FTIR spectra of CNTs and f-CNTs are presented in Fig. 1. The spectrum of CNTs shows peaks at 3440 and 1636 cm^{-1} , which can be assigned to O–H stretching vibrations and double bonds C=C of aromatic rings, respectively. After treatment, a peak at 1720 cm^{-1} was observed for f-CNTs, which is related to the (O=C–OH) stretching vibrations in the carboxylic acid group [50]. This confirms that the carboxyl groups were grafted on CNT surface during the oxidation process.

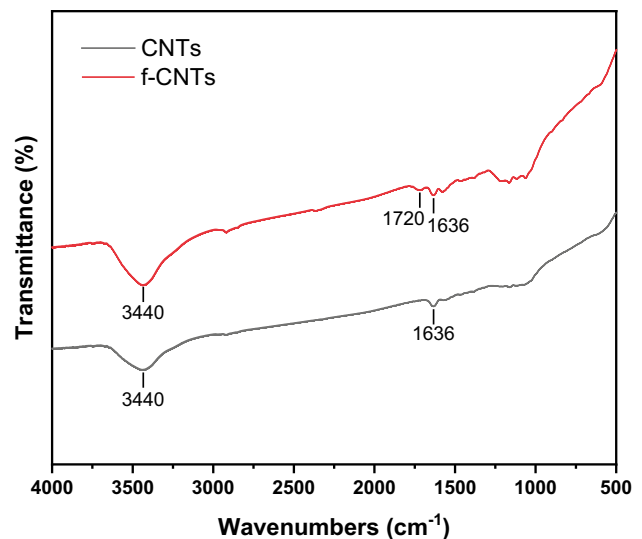


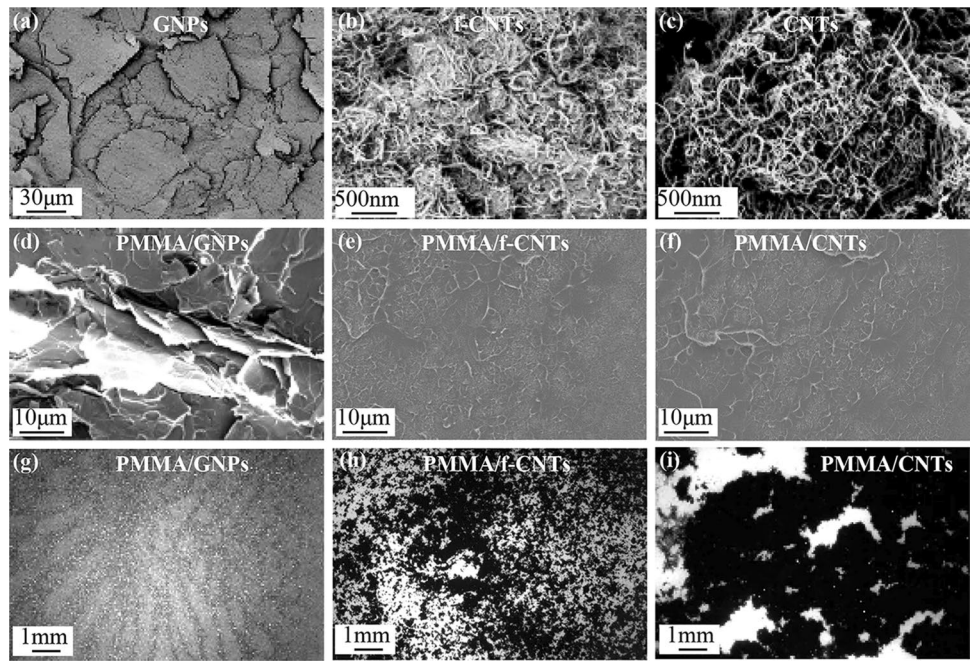
Fig. 1 FTIR spectra of CNTs and f-CNTs

The morphologies of conductive fillers used in this study are shown in Fig. 2a–c. The diameter of the pristine GNPs (Fig. 2a) is several tens of microns, which is in agreement with the statement of the manufacturer. It is also stated that the GNPs are about 10 layers thick, e.g., several nanometers in thickness. Thus, the GNPs have a very high aspect ratio (> 1000). Figure 2b, c show the presence of smaller aggregates and tangled CNT clusters. However, Fig. 2b shows shorter length of the f-CNTs than the CNTs in Fig. 2c after treatment with acids [51]. Figure 2d–f show the cross-section of the binary composite films PMMA/GNPs, PMMA/f-CNTs, and PMMA/CNTs, respectively. The rough fracture surface in Fig. 2d indicates poor interfacial adhesion between the larger-sized GNPs and the PMMA matrix. In contrast, the smaller-sized f-CNTs and CNTs were well embedded in the matrix, leading to a much smoother surface. The macroscopic distribution of fillers in the polymer is shown in Fig. 2g–h. PMMA/GNPs showed obvious GNPs phase segregation due to the poor compatibility between GNPs and PMMA matrix [52]. f-CNTs were more uniformly and randomly dispersed, while pristine CNTs formed much larger aggregates. This confirms the improvement in the compatibility via chemical functionalization. The functional group of the f-CNTs could react with an active group on the polymer chains of the PMMA; thus, they will enhance the distribution of the fillers into the polymer matrix.

3.2 Electrical properties of the binary composite films

The logarithm of the in-plane ($\log \sigma_r$) and perpendicular conductivity ($\log \sigma_p$) as a function of the filler volume

Fig. 2 SEM images of the conductive fillers: **a** GNPs; **b** f-CNTs; **c** CNTs used in this study. SEM images of the cross-section of the binary composite films at 0.005 filler loading: **d** PMMA/GNPs; **e** PMMA/f-CNTs; **f** PMMA/CNTs. Optical images of the surface of the binary composite films at 0.005 filler loading: **g** PMMA/GNPs; **h** PMMA/f-CNTs; **i** PMMA/CNTs



fraction for the binary composite films are shown in Fig. 3. The dots represent the experimental data. It can be seen when the filler loading exceeds a certain amount, the electrical conductivity increases significantly. This special filler content is called percolation threshold (Φ_c). Φ_c in this work was determined by the general effective medium (GEM) theory equation [53] and confirmed by the classical percolation theory equation [54]. GEM equation is

$$(1 - \Phi) \frac{\sigma_m / s - \sigma_c / s}{\sigma_m / s + \frac{1 - \Phi_c}{\Phi_c} \cdot \sigma_c / s} + \Phi \frac{\sigma_f / t - \sigma_c / t}{\sigma_f / t + \frac{1 - \Phi_c}{\Phi_c} \cdot \sigma_c / t} = 0 \quad (3)$$

where σ_m , σ_c , and σ_f are the conductivities of the PMMA matrix, the composite, and the filler, respectively. Φ is the volume fraction of fillers, and Φ_c is the percolation threshold. The values of the exponents and t are generally taken to be 0.87 and 2, respectively.

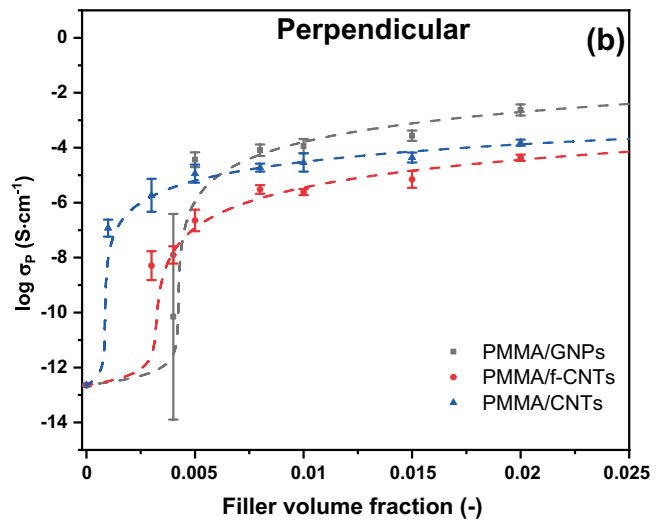
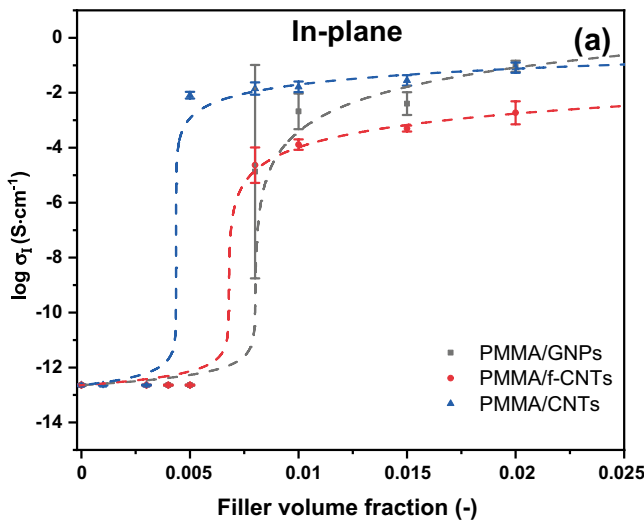


Fig. 3 The logarithm of the **a** in-plane and **b** perpendicular conductivity as a function of filler volume fraction for PMMA/GNP, PMMA/f-CNT, and PMMA/CNT composite films. The dashed lines

show the best fit utilizing the GEM Eq. 3 with two adjustable parameters (Φ_c and exponent t in Eq. 3)

The classical equation is

$$\sigma = \sigma_0(\Phi - \Phi_c)^f \quad (4)$$

where σ and σ_0 are the conductivities of the composite and the electrical filler, respectively. Φ is the volume fraction of fillers, and Φ_c is the percolation threshold. For filler concentrations of composites with $\Phi > \Phi_c$, the experimental results are fitted by plotting $\log \sigma$ against $\log(\Phi - \Phi_c)$ and Φ_c has been adjusted to obtain the best linear fit.

The dashed lines in Fig. 3 are the fitting results using GEM Eq. 3 while those in Fig. S2 are the fitting results using classical Eq. 4. Binary PMMA/f-CNTs had a conductivity of 1–2 orders of magnitude lower than PMMA/CNTs due to the functional process which added defects to the CNTs and reduced the aspect ratio [55]. Another possibility is that the interaction of PMMA with f-CNTs formed an insulating layer on filler's surface, which made the tunneling of electrons from tube to tube more difficult [56, 57]. The $\log \sigma_I$ of PMMA/CNTs was higher than that of PMMA/GNPs beyond both Φ_c , while the $\log \sigma_P$ was opposite. It can also be seen that the conductivity of PMMA/GNP composite was more fluctuant in the percolation region and it also showed a narrower insulator–conductor transition region than PMMA/f-CNTs and PMMA/CNTs, which was related to the worse distribution and dispersion of the GNPs [58]. This means PMMA/GNPs were more sensitive to small changes in the filler concentration and had worse stability of electrical properties. The corresponding in-plane ($\Phi_{c,I}$) and perpendicular percolation thresholds ($\Phi_{c,P}$) predicted from Eq. 3 are shown in Table 1. Both $\Phi_{c,I}$ and $\Phi_{c,P}$ followed the sequence of PMMA/GNPs > PMMA/f-CNTs > PMMA/CNTs. PMMA/CNT composite had the lowest percolation threshold among the three kinds of binary composites. This indicates that the large aggregates and poor distribution of CNTs in Fig. 2 facilitated the formation of conductive networks [59].

3.3 Synergy in in-plane electrical properties

The investigation on the synergistic effect of hybrid fillers on the electrical properties of CPCs was conducted on ternary PMMA/GNP/f-CNT and PMMA/GNP/CNT composites

comprising a total volume fraction of hybrid fillers between 0.005 (close to the Φ_c of binary composites) to 0.02 (near-saturated concentration of perpendicular conductivity). The synergy in the in-plane direction is shown in contour plot diagrams in Fig. 4, where the X-axis corresponds to GNP volume fraction and Y-axis corresponds to f-CNTs or CNT volume fraction. The black dots represent the experimental data, which generated the black iso-contour lines connecting points of equal $\log \sigma$ value. To define the synergy region and the strongest synergy points, data for composites with the same total filler content were connected by a blue dashed line, which means the total filler volume fraction in each blue dash line is kept constant. These lines are parallel to each other. For clarity, only some of the tangents to the iso-lines are shown in the contour plot diagrams. The strongest synergy points (white circles) are the contact points of these blue lines and iso-lines, which reveal a ternary recipe with the most possible reduction of the total volume fraction as compared to the binary systems [16]. These circles were connected by a white line, indicating a trajectory of the strongest synergy at certain filler volume fractions.

The aforementioned type 3 synergy is fulfilled when the conductivity of any point in the same blue line (ternary composite) is higher than the points in the X- and Y-axes (binary composite). From the contour lines of Fig. 4a, it can be observed that when the filler fraction in PMMA was less than about 0.01, type 3 synergy happened, but at higher filler contents, only type 2 synergy or even anti-synergy existed. The region of synergy and non-synergy is distinguished by the bright and the shadow part in Fig. 4 as well as in the following contour plot diagrams. The strongest synergy occurred at a total filler fraction between 0.003 and 0.005 and at GNP/f-CNT ratio of about 1/1. For example, at the point of 0.0025 GNPs + 0.0025f-CNTs, the value of $\log \sigma_I$ was -4.56 , which was 8 orders of magnitude higher than both the insulating binary CPCs. In the case of PMMA/GNP/CNT composite (Fig. 4b), in contrast to PMMA/GNPs/f-CNTs, type 3 synergy was fulfilled when filler fractions were more than 0.01. This phenomenon has also been found in other research [60].

To better understand the synergy in the in-plane conductivity as well as the effect of hybrid fillers on the percolation behavior of CPCs, the $\log \sigma_I$ as a function of the total filler

Table 1 In-plane and perpendicular percolation thresholds of the binary composites and ternary composites obtained from Eq. 3

	PMMA/GNPs	PMMA/f-CNTs	PMMA/CNTs	PMMA/GNPs/f-CNTs(2/1)	PMMA/GNPs/CNTs(1/1)
$\Phi_{c,I}$	0.008 ± 0.0025	0.0068 ± 0.0025	0.0044 ± 0.0017	0.0041 ± 0.0013 0.0076 ± 0.0025 *	0.0048 ± 0.0017 0.0062 ± 0.0021 *
$\Phi_{c,P}$	0.0042 ± 0.0013	0.0031 ± 0.00085	0.00084 ± 0.00095	0.0024 ± 0.00045 0.0038 ± 0.0011 *	0.00057 ± 0.00036 0.0025 ± 0.0011 *

*Values predicted from Eq. 1 according to Φ_c of the binary composite

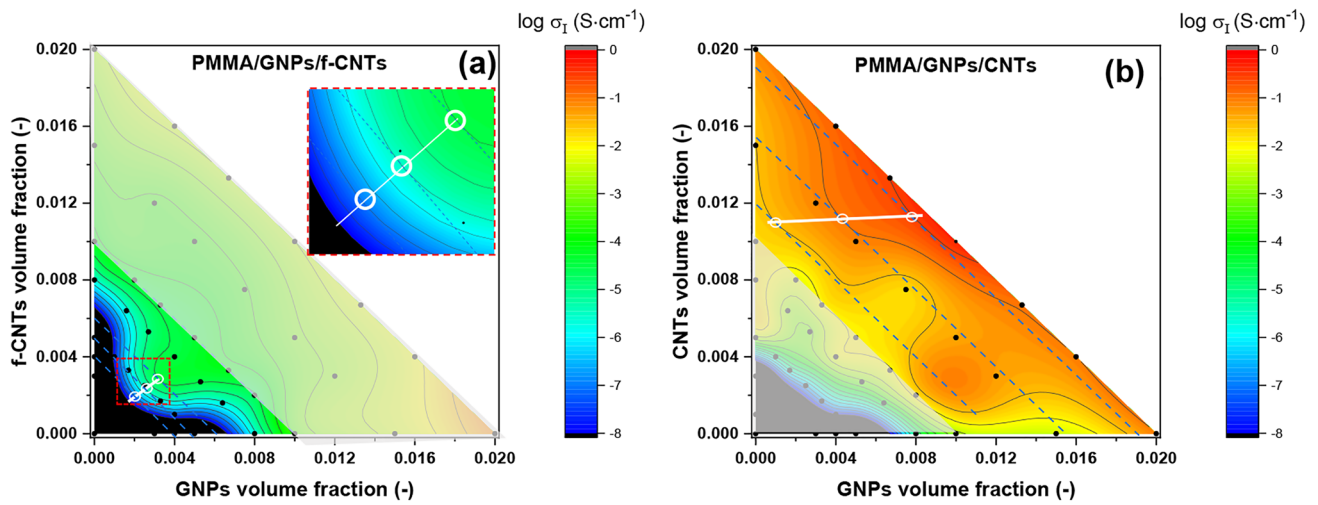


Fig. 4 The logarithmic value of in-plane conductivity of **a** PMMA/GNP/f-CNT composite and **b** PMMA/GNP/CNT composite versus filler volume fraction of two hybrid fillers in a contour plot diagram

showing synergy region and strongest synergy points (white circles and white line). The contour interval is 0.5. The inset is a magnified view of the strongest synergy points

volume fraction of ternary systems and binary systems is shown in Fig. 5, where GNPs/f-CNTs of 2/1 and GNPs/CNTs of 1/1 were chosen to present the ternary CPCs. The values of the percolation threshold could also be found in Table 1. With the addition off-CNTs, the percolation threshold of ternary PMMA/GNPs/f-CNTs decreased from 0.008 ± 0.0025 to 0.0041 ± 0.0013 , which was also lower than the predicted value (0.0076 ± 0.0025) from Eq. 1 based on the $\Phi_{c,l}$ of PMMA/GNP and PMMA/f-CNT composites. Therefore, type 4 synergy was achieved in this ternary composite. Moreover, the conductivity of ternary PMMA/

GNPs/f-CNTs was higher than both binary composites below the total filler fraction of 0.01. However, as discussed before, the synergy in conductivity did not occur above that filler content. The conductivity of ternary composites became only a little higher than that of binary PMMA/f-CNTs but kept around 1 order of magnitude lower than that of PMMA/GNPs. This indicates that the combination of GNPs and f-CNTs facilitated the formation of in-plane conductive networks, but the electrical conductivity was dominated by the weaker conductive f-CNTs. This might be attributed to the 25-mm-long measuring distance of in-plane

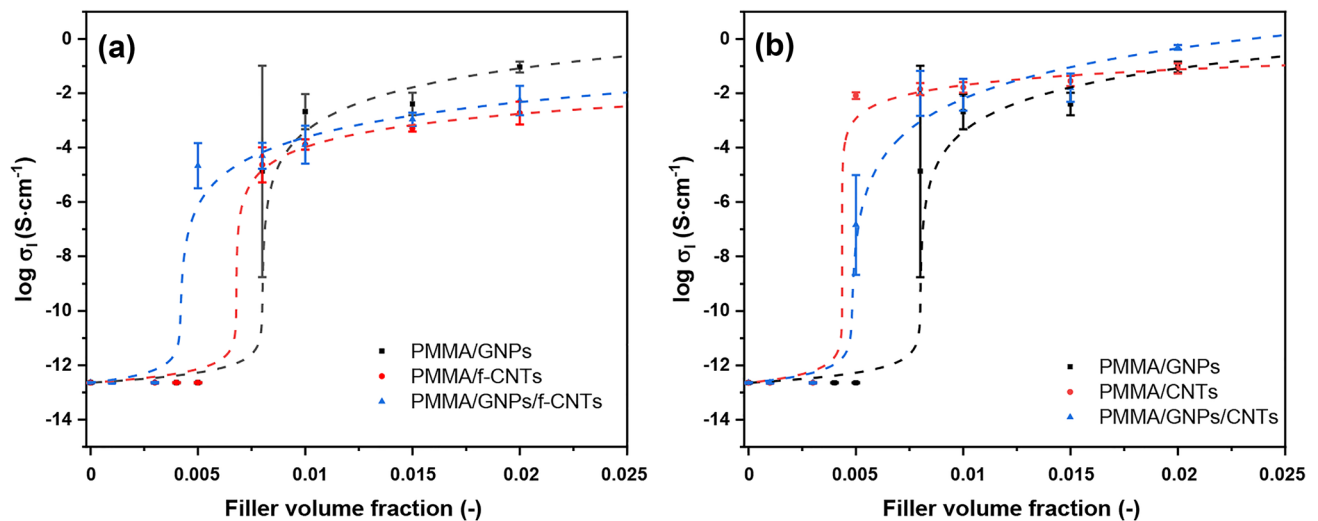


Fig. 5 Comparison of the logarithm of the in-plane conductivity as a function of the filler volume fraction of ternary system and binary system: **a** Ternary PMMA/GNPs/f-CNTs, binary PMMA/GNP, and

PMMA/f-CNTs. **b** Ternary PMMA/GNPs/CNTs, binary PMMA/GNPs, and PMMA/CNTs

direction, where the complete conductive paths were comprised of GNP-GNP, GNP-f-CNT, and f-CNT-f-CNT junctions. The GNP-f-CNT and f-CNT-f-CNT junctions limited the improvement of $\log \sigma_I$. In Fig. 5b, PMMA/GNPs had the highest $\Phi_{c,I}$ and lowest $\log \sigma_I$ independent of GNP concentration. Composite filled with hybrid GNPs and CNTs had a $\Phi_{c,I}$ of 0.0048 ± 0.0017 , which was close to PMMA/CNTs (0.0044 ± 0.0017) and lower than the predicted one (0.0062 ± 0.0021). Type 4 synergy was achieved in PMMA/GNP/CNT system likewise. As to the conductivity, $\log \sigma_I$ near $\Phi_{c,I}$ was lower but grew faster with total filler content increasing, surpassing the conductivities of both binary composites beyond 0.01 filler loading. This phenomenon is likely resulted from the formation of more conductive paths in the in-plane direction due to the homogenous distribution of fillers as shown in Fig. S3e.

The synergy in percolation could be explained by the corresponding macroscopic distribution of the two kinds of hybrid fillers in PMMA as shown in Fig. 6a, b. Compared to the binary system in Fig. 2g, the GNP segregation disappeared in the hybrid GNP/f-CNT system (Fig. 6a); a more homogeneous distribution was achieved. It also shows more continuous networks than both binary composites. As discussed before, f-CNTs were better dispersed than CNTs; however, the electrical properties of binary PMMA/f-CNTs were poorer than that of PMMA/CNTs due to the detrimental effect of the functionalization. For these ternary systems, f-CNTs with better compatibility with polymer matrix could also improve the dispersion of GNPs into PMMA. Due to the improved dispersion state and large aspect ratio of GNPs, it became easier for hybrid fillers to connect each other. For GNP/CNT system (Fig. 6b), the segregation of GNPs also vanished and the hybrid fillers tended to distribute like single CNTs but the aggregations were slightly smaller. That is

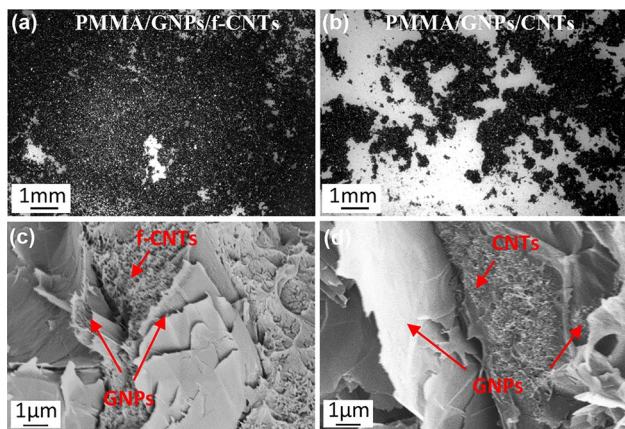


Fig. 6 Optical images of the surface of the **a** PMMA/GNP/f-CNT and **b** PMMA/GNP/CNT composite films at 0.005 total filler loading. SEM image showing intercalation of **c** f-CNTs and **d** CNTs between GNPs

why the ternary PMMA/GNPs/CNTs exhibited lower conductivity at a filler fraction below 0.01. Figure 6c, d show that both f-CNTs and CNTs could embed GNPs and bridge the graphene layers into a 3-D interconnected structure at a nano-scale. It can be inferred that although 3-D interconnected pathways formed in both ternary systems, the in-plane conductivity was more dependent on the macroscopic distribution state of fillers.

3.4 Synergy in perpendicular electrical properties

The synergistic effects of GNPs/f-CNTs and GNPs/CNTs on $\log \sigma_p$ of the ternary CPCs are shown in Fig. 7. Because the sequence of $\log \sigma_p$ of the binary CPCs followed PMMA/GNPs > PMMA/CNTs > PMMA/f-CNTs beyond 0.005 filler loading, type 3 synergy of ternary systems can be clarified by comparison to the PMMA/GNPs. The result shows that it occurred when GNPs/f-CNTs > 2/1 and GNPs/CNTs > 1/4 approximately for PMMA/GNP/f-CNT composite and PMMA/GNP/CNT composite, respectively. It can also be noted, unlike the filler loading-determined $\log \sigma_p$, $\log \sigma_p$ was more dependent on the filler ratio. The strongest synergy points were close to the filler ratio of 4/1 and 2/1 for PMMA/GNP/f-CNT and PMMA/GNP/CNT composite, respectively.

Typically, $\log \sigma_p$ of ternary and binary CPCs as a function of the filler volume fraction is shown in Fig. 8, where GNP/f-CNT was 2/1 and GNP/CNT was 1/1 in the ternary system. In Fig. 8a, the $\Phi_{c,p}$ of PMMA/GNP/f-CNT composite decreased from 0.0042 ± 0.0013 (PMMA/GNPs) or 0.0031 ± 0.00085 (PMMA/f-CNTs) to 0.0024 ± 0.00045 . In comparison to the predicted $\Phi_{c,p}$ of 0.0038 ± 0.0011 , type 4 synergy was realized. The $\Phi_{c,I}$ of ternary composites is lower than both binary composites, which has also been found in other reports [24, 61]. Interestingly, unlike the $\log \sigma_I$ discussed in the last section, the $\log \sigma_p$ of ternary composites was very close to that of binary PMMA/GNPs rather than be limited by f-CNTs, indicating that the conductive pathways through-thickness were dominated by GNPs. This could be explained in two aspects. First, the thickness of films was rather small (about 0.2 mm) relative to the sample length, GNPs with a d_{50} as an index of 50 μm could form the conductive networks easily across this distance, and the contribution of less conductive and short f-CNTs (1- μm length) could be neglected. Second, one-third of the GNPs was replaced by f-CNTs in this hybrid system, but the conductivity of the ternary composite could remain at a comparable level as PMMA/GNP composite. Apparently, f-CNTs with 2 orders of magnitude lower conductivity could not compensate for the loss if GNPs kept the original exfoliation state. Therefore, the main reason is a more effective exfoliation of GNPs in the presence of CNTs. As to PMMA/GNPs/CNTs, the $\Phi_{c,I}$ was 0.00057 ± 0.00036 , even lower than that of PMMA/CNT composite (0.00084 ± 0.00095).

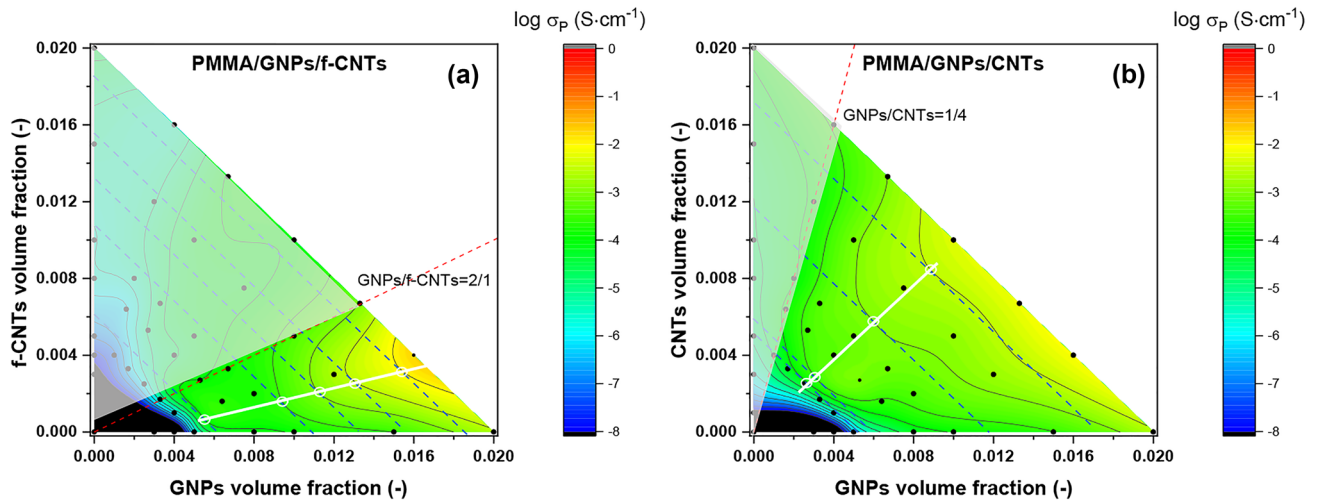


Fig. 7 The logarithmic value of perpendicular conductivity of **a** PMMA/GNP/f-CNT composite and **b** PMMA/GNP/CNT composite versus filler volume fraction of two hybrid fillers in a contour plot

diagram showing synergy region and strongest synergy points (white circles and white line). The contour interval is 0.5

The predicted one was 0.0025 ± 0.0011 ; type 4 synergy was also achieved. Furthermore, the $\log \sigma_p$ was higher than both binary composites at all filler contents, which can also be obtained in the contour plot diagram in Fig. 7b. This could also be ascribed to the bridging and the intercalation of CNTs between the GNPs stacks. Since GNPs and CNTs both had high and close conductivities, the synergistic effect of this pair was more remarkable than GNPs/f-CNTs.

It could be observed from Fig. 7, filler ratio played an important role in the electrical conductivity of ternary composites, and the synergy region of PMMA/

GNPs/f-CNTs was narrower than that of PMMA/GNPs/CNTs due to the large difference in conductivities of GNPs and f-CNTs. To better understand the relation between the perpendicular conductivity and filler ratio, a contour plot diagram of the PMMA/GNP/f-CNT composite was further analyzed in Fig. 9, which shows the synergistic behavior evolution with filler volume ratios varying by four regions. This could be interpreted combining with the microstructural conductive network evolution with the volume ratio of GNPs/f-CNTs, which is shown in the schematic diagram Fig. 10.

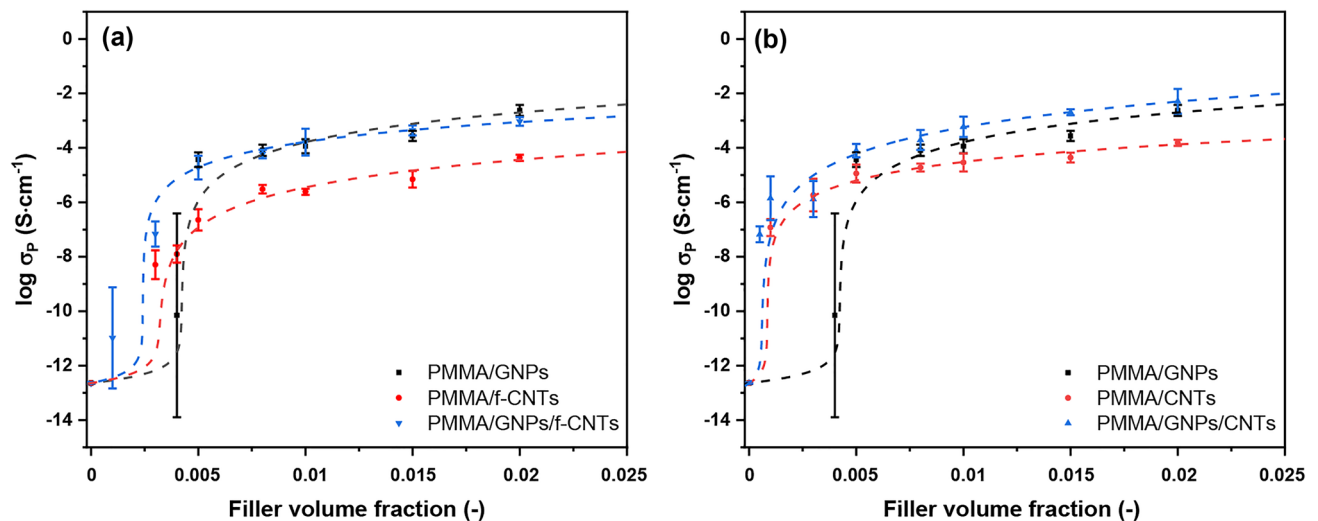
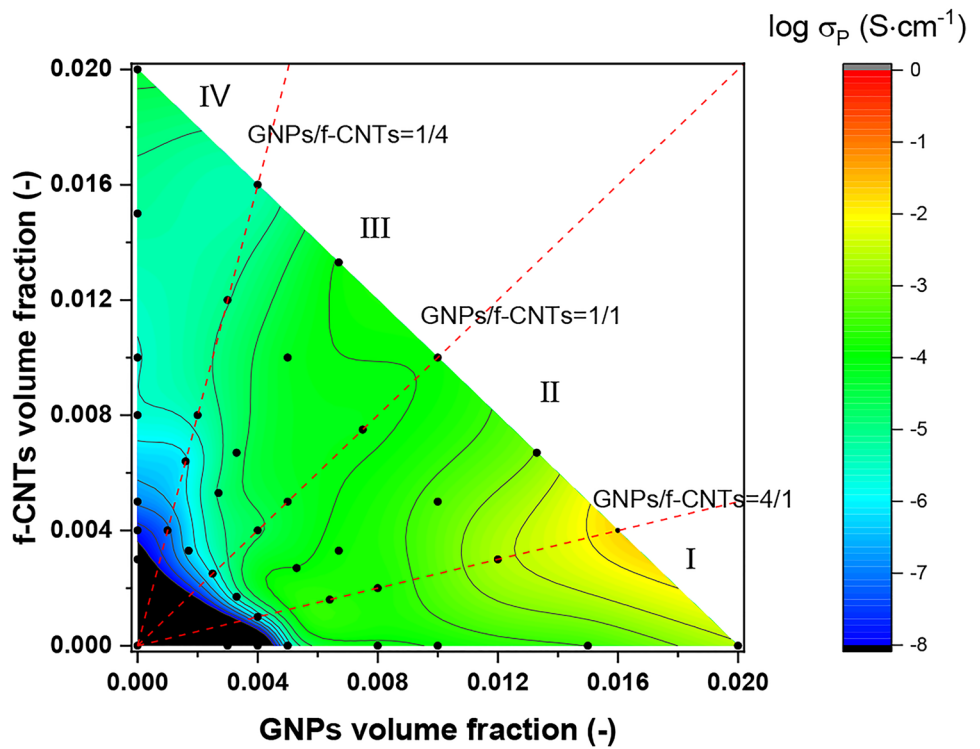


Fig. 8 Comparison of the logarithm of the perpendicular conductivity as a function of the filler volume fraction of ternary system and binary system: **a** ternary PMMA/GNPs/f-CNTs, binary PMMA/

GNPs, and PMMA/f-CNTs. **b** Ternary PMMA/GNPs/CNTs, binary PMMA/GNPs, and PMMA/CNTs

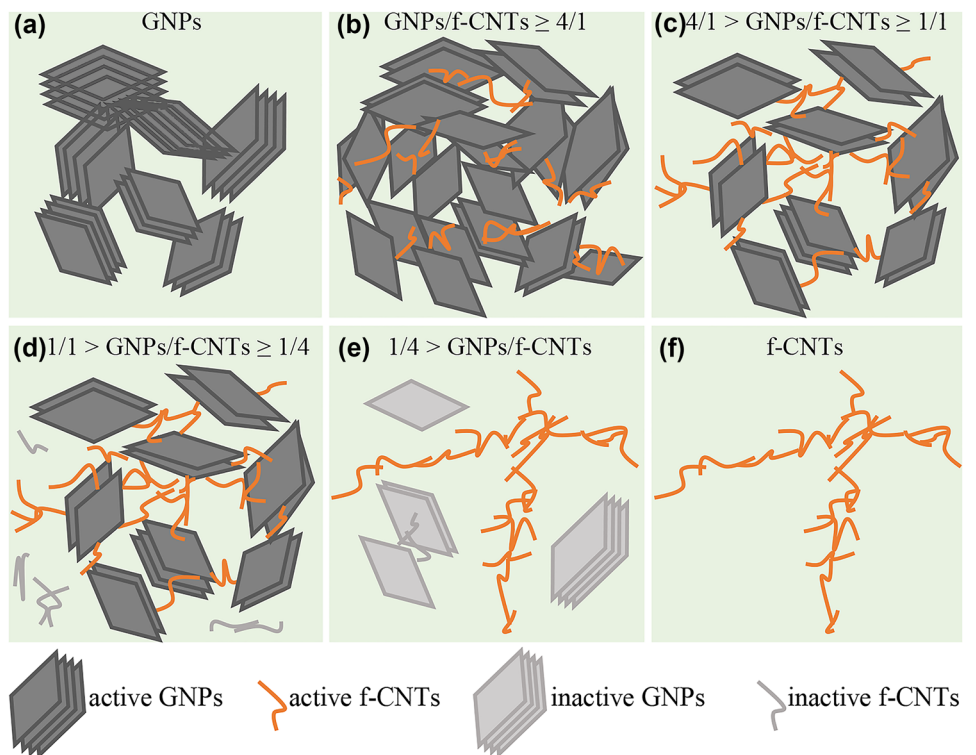
Fig. 9 The logarithmic value of perpendicular conductivity of PMMA/GNP/f-CNT composite versus filler volume fraction of two hybrid fillers in a contour plot diagram showing the different synergistic behavior evolution at different regions of filler volume ratios. The contour interval is 0.5



I: $\text{GNPs}/\text{f-CNTs} \geq 4/1$, compared to the PMMA/GNP composite, a rise of approximately one order of magnitude in the $\log \sigma_p$ can be observed for the ternary composite. The strongest synergy points were located in this region as

well as shown in Fig. 7a. This is attributed to the intercalation of f-CNTs between the GNP stacks. With the exfoliation of GNPs, the dispersion changed from Fig. 10a to b. The looser-dispersed and well-connected GNPs not only

Fig. 10 Schematic diagram of the microstructural conductive network evolution in PMMA/GNP/f-CNT composites with the volume ratio of GNPs/f-CNTs decreasing for interpreting the different synergistic behaviors. CPCs comprising **a** single GNPs, **b** $\text{GNPs}/\text{f-CNTs} \geq 4/1$, **c** $4/1 > \text{GNPs}/\text{f-CNTs} \geq 1/1$, **d** $1/1 > \text{GNPs}/\text{f-CNTs} \geq 1/4$, **e** $1/4 > \text{GNPs}/\text{f-CNTs}$, and **f** single f-CNTs



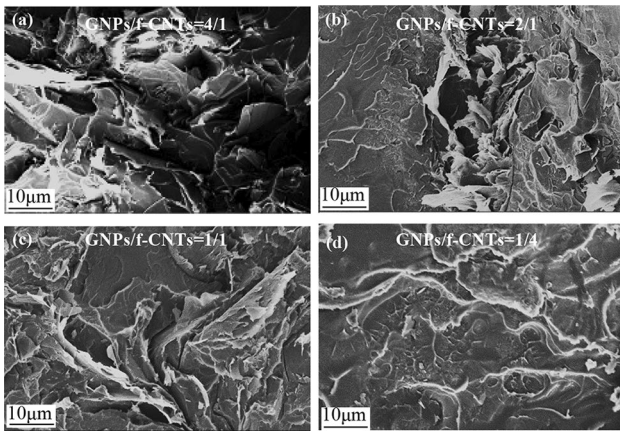


Fig. 11 SEM images of the cross section of the ternary PMMA/GNP/f-CNT composite films at 0.005 filler loading: **a** GNPs/f-CNTs = 4/1; **b** GNPs/f-CNTs = 2/1; **c** GNPs/f-CNTs = 1/1; **d** GNPs/f-CNTs = 1/4

increased the conductive pathways, but also remain the high conductivity by GNP-GNP connection.

II: $4/1 > \text{GNPs/f-CNTs} \geq 1/1$, $\log \sigma_p$ did not rise further with the f-CNTs increasing, it dropped back to or even lower than the value of PMMA/GNPs. The corresponding microstructural conductive networks might be: GNPs gradually lost contact with each other and connected with some f-CNT clusters instead to form the conductive networks (Fig. 10c). Therefore, the $\log \sigma_p$ decreased due to the lower conductivity of f-CNTs.

III: $1/1 > \text{GNPs/f-CNTs} \geq 1/4$, if the volume fraction of f-CNTs increased while that of GNPs kept a constant, the near-vertical contour lines in this region just revealed that

the $\log \sigma_p$ almost kept a constant. The structural transformation can be seen from Fig. 10c to d. Additional f-CNTs did not play a role in the charge transport, as shown by the inactive f-CNTs.

IV: $1/4 > \text{GNPs/f-CNTs}$, the ternary CPCs exhibited a similar conductivity to the binary PMMA/f-CNT composite at the same total filler concentration, e.g., the almost horizontal in this region. This could be illustrated by Fig. 10e; the inactive GNPs did not connect with the f-CNT conductive networks; thus, this small number of GNPs did not contribute to the conductivity of ternary composites, either. The representative of the morphologies of ternary CPCs in each region is shown in Fig. 11, which are also in agreement with the schematic diagram in Fig. 10b–e, while Fig. 10a and f are corresponding to the morphologies of binary CPCs as shown in Fig. 2d and e, respectively.

3.5 Conductivity anisotropy

As discussed above, the synergies in the in-plane and perpendicular direction of CPC films were mainly determined by the total filler volume fraction and volume ratio between the two fillers, respectively. Moreover, due to the significant difference in the measuring distances of the two directions and that in the conductivities of f-CNTs and CNTs, the two kinds of ternary CPCs showed different levels of enhancement of $\log \sigma_l$ and $\log \sigma_p$. The conductivity anisotropy at various ratios of the filler volume fractions was thus investigated as shown in Fig. 12. The conductivity anisotropy was defined as the ratio of the in-plane conductivity to perpendicular conductivity, as given by the following equation:

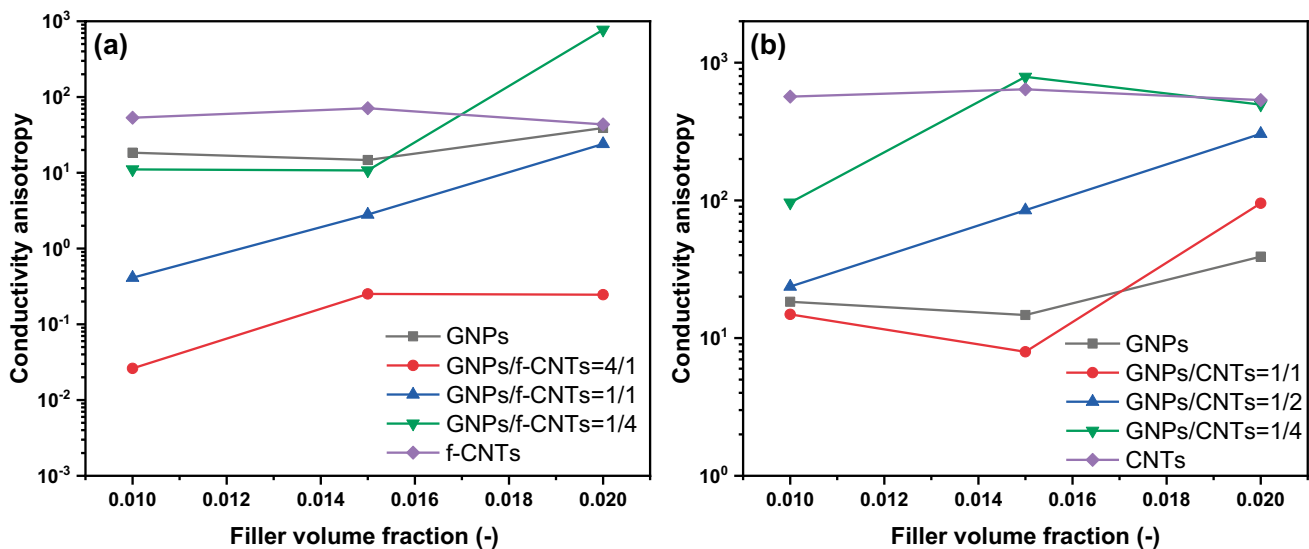


Fig. 12 Conductivity anisotropy of composite films as a function of total filler volume fraction: **a** PMMA/GNP/f-CNT composite and **b** PMMA/GNP/CNT composite

$$\text{Anisotropy} = \sigma_I / \sigma_P \quad (5)$$

In Fig. 12a, PMMA comprising single GNPs or f-CNTs showed an anisotropy of 10–100, indicating the influence of the single filler in the both directions. Interestingly, the CPCs filled with hybrid GNPs/f-CNTs showed a wide span of anisotropy almost from 0.01 to 1000 when the ratio of GNPs/f-CNTs decreased from 4/1 to 1/4. As discussed before, the $\log \sigma_I$ of ternary CPCs almost kept a value close to that of PMMA/f-CNTs regardless of the filler ratio, while the $\log \sigma_P$ decreased with the ratio of GNPs/f-CNTs decreasing. The result gives a new revelation of tuning the electrical conductivity anisotropy: hybridizing two conductive fillers of different conductivities but similar anisotropy: one of which dominates the in-plane conductivity while the other dominates the perpendicular conductivity. With the variation of filler ratio and content, various conductive structures could be constructed. The wide range of anisotropy also concludes 1, e.g., isotropic conductive composite. Compared to PMMA/f-CNTs or PMMA/GNPs, PMMA/CNTs exhibited a higher anisotropy as shown in Fig. 12b. The anisotropy of ternary PMMA/GNP/CNT composite was between the two corresponding binary CPCs and increased with the ratio of GNPs/CNTs decreasing. It reveals another strategy of the tunable anisotropy: combining two conductive fillers of close conductivities but different anisotropy, anisotropy between two single filler systems could be obtained. Overall, the anisotropy of all CPCs increased with the total filler content, which might be attributed to the increase in filler orientation in the in-plane direction [62, 63].

4 Conclusions

Pristine CNTs and functionalized CNTs (f-CNTs) were respectively added into the PMMA/GNP composites, and their synergistic effects on the electrical properties were investigated. By establishing efficient 3-D interconnected conductive paths in the ternary composite, synergies in both the in-plane and perpendicular direction were achieved. In the in-plane direction, due to the lower conductivity but better dispersion of the f-CNTs relative to the CNTs, PMMA/GNP/f-CNT composite showed synergy behaviors below a filler fraction of 0.01, while PMMA/GNPs/CNTs showed synergistic effects beyond this filler loading. In the perpendicular direction, the synergy behaviors of both ternary composites were more dependent on the filler ratios, a schematic diagram of the evolution of the 3-D conductive pathways of PMMA/GNP/f-CNT composite at different GNP/f-CNT ratios was presented to explain their contribution to the charge transport. Moreover, the conductivity anisotropy can be tailored by constructing different conductive structures at different filler loadings or ratios. In this work, an anisotropy was achieved of

approximately from 0.01 to 1000 and 10 to 1000 in PMMA/GNP/f-CNT and PMMA/GNP/CNT composite, respectively. The results open up a new way to design promising highly anisotropic or isotropic CPCs.

Supplementary Information The online version contains supplementary material available at <https://doi.org/10.1007/s42114-021-00332-y>.

Acknowledgements The authors would like to thank Jennifer Reiser from Institute of Polymer Materials (Friedrich-Alexander-University Erlangen-Nuremberg), for the FTIR measurement guidance.

Funding Open Access funding enabled and organized by Projekt DEAL.

Declarations

Conflict of interest The authors declare no competing interests.

Open Access This article is licensed under a Creative Commons Attribution 4.0 International License, which permits use, sharing, adaptation, distribution and reproduction in any medium or format, as long as you give appropriate credit to the original author(s) and the source, provide a link to the Creative Commons licence, and indicate if changes were made. The images or other third party material in this article are included in the article's Creative Commons licence, unless indicated otherwise in a credit line to the material. If material is not included in the article's Creative Commons licence and your intended use is not permitted by statutory regulation or exceeds the permitted use, you will need to obtain permission directly from the copyright holder. To view a copy of this licence, visit <http://creativecommons.org/licenses/by/4.0/>.

References

- Xie L, Zhu Y (2018) Tune the phase morphology to design conductive polymer composites: A review. *Polym Compos* 39:2985–2996. <https://doi.org/10.1002/pc.24345>
- Mir SM, Jafari SH, Khonakdar HA, Krause B, Pötschke P, Taheri Qazvini N (2016) A promising approach to low electrical percolation threshold in PMMA nanocomposites by using MWCNT-PEO pre-dispersions. *Mater Des* 111:253–262. <https://doi.org/10.1016/j.matdes.2016.08.073>
- Xu H, Schubert DW (2020) Electrical conductivity of polystyrene/poly (n-alkyl methacrylate) s/carbon nanotube ternary composite casting films. *J Polym Res* 27:153
- Hafez IH, Berber MR (2016) Carbon nanotubes—current progress of their polymer composites. *IntechOpen*
- Guo J, Li X, Liu H, Young DP, Song G, Song K, Zhu J, Kong J, Guo Z (2021) Tunable magnetoresistance of core-shell structured polyaniline nanocomposites with 0-, 1-, and 2-dimensional nanocarbons. *Adv Compos Hybrid Mater* 4:51–64. <https://doi.org/10.1007/s42114-021-00211-6>
- Xie M, Zhang Y, Krašný MJ, Bowen C, Khanbareh H, Gathercole N (2018) Flexible and active self-powered pressure, shear sensors based on freeze casting ceramic-polymer composites. *Energy Environ Sci* 11:2919–2927. <https://doi.org/10.1039/c8ee01551a>
- Naz A, Kausar A, Siddiq M, Choudhary MA (2016) Comparative review on structure, properties, fabrication techniques, and relevance of polymer nanocomposites reinforced with carbon nanotube and graphite fillers. *Polym - Plast Technol Eng* 55:171–198. <https://doi.org/10.1080/03602559.2015.1055504>

8. Wei H, Li A, Kong D, Li Z, Cui D, Li T, Dong B, Guo Z (2021) Polypyrrole/reduced graphene aerogel film for wearable piezoresistive sensors with high sensing performances. *Adv Compos Hybrid Mater* 4:86–95. <https://doi.org/10.1007/s42114-020-00201-0>
9. Zhang C, Zhang Y, Hao X, Liu H, Lv X, Zhu J, Han W, Zhang Y (2018) Fabrication of reduced graphene oxide/chitosan composite fiber by dry-jet wet spinning. *Adv Compos Hybrid Mater* 1:347–355. <https://doi.org/10.1007/s42114-018-0029-2>
10. Paszkiewicz S, Szymczyk A, Sui XM, Wagner HD, Linares A, Ezquerro TA, Roslaniec Z (2015) Synergetic effect of single-walled carbon nanotubes (SWCNT) and graphene nanoplatelets (GNP) in electrically conductive PTT-block-PTMO hybrid nanocomposites prepared by in situ polymerization. *Compos Sci Technol* 118:72–77. <https://doi.org/10.1016/j.compscitech.2015.08.011>
11. Qu M, Nilsson F, Qin Y, Yang G, Pan Y, Liu X, Rodriguez GH, Chen J, Zhang C, Schubert DW (2017) Electrical conductivity and mechanical properties of melt-spun ternary composites comprising PMMA, carbon fibers and carbon black. *Compos Sci Technol* 150:24–31
12. Atif R, Inam F (2016) Reasons and remedies for the agglomeration of multilayered graphene and carbon nanotubes in polymers. *Beilstein J Nanotechnol* 7:1174–1196. <https://doi.org/10.3762/bjnano.7.109>
13. Wang BaoMin, Zhao R (2018) Dispersion of graphene in aqueous solution. *Russ J Phys Chem A* 92:1558–1562. <https://doi.org/10.1134/S003602441808006X>
14. Szeluga U, Kumanek B, Trzebicka B (2015) Synergy in hybrid polymer/nanocarbon composites. A review. *Compos Part A Appl Sci Manuf* 73:204–231. <https://doi.org/10.1016/j.compositesa.2015.02.021>
15. Li Y, Huang X, Zeng L, Li R, Tian H, Fu X, Wang Y, Zhong WH (2019) A review of the electrical and mechanical properties of carbon nanofiller-reinforced polymer composites. *J Mater Sci* 54:1036–1076. <https://doi.org/10.1007/s10853-018-3006-9>
16. Qu M, Nilsson F, Schubert DW (2019) Novel definition of the synergistic effect between carbon nanotubes and carbon black for electrical conductivity. *Nanotechnology* 30:245703
17. Yang G, Schubert DW, Nilsson F, Qu M, Redel M (2020) A study of a novel synergy definition for ternary CB/CNT composites suggesting a representative model for CB and CNT. *Macromol Theory Simulations* 29:2000035
18. Liu H, Gao J, Huang W, Dai K, Zheng G, Liu C, Shen C, Yan X, Guo J, Guo Z (2016) Electrically conductive strain sensing polyurethane nanocomposites with synergistic carbon nanotubes and graphene bifillers. *Nanoscale* 8:12977–12989. <https://doi.org/10.1039/c6nr02216b>
19. Maiti S, Shrivastava NK, Suin S, Khatua BB (2013) Polystyrene/MWCNT/graphite nanoplate nanocomposites: Efficient electromagnetic interference shielding material through graphite nanoplate-MWCNT-graphite nanoplate networking. *ACS Appl Mater Interfaces* 5:4712–4724. <https://doi.org/10.1021/am400658h>
20. Hu H, Zhao L, Liu J, Liu Y, Cheng J, Luo J, Liang Y, Tao Y, Wang X, Zhao J (2012) Enhanced dispersion of carbon nanotube in silicone rubber assisted by graphene. *Polymer (Guildf)* 53:3378–3385. <https://doi.org/10.1016/j.polymer.2012.05.039>
21. Al-Saleh MH (2015) Electrical and mechanical properties of graphene/carbon nanotube hybrid nanocomposites. *Synth Met* 209:41–46. <https://doi.org/10.1016/j.synthmet.2015.06.023>
22. Tang Y, Gou J (2010) Synergistic effect on electrical conductivity of few-layer graphene/multi-walled carbon nanotube paper. *Mater Lett* 64:2513–2516. <https://doi.org/10.1016/j.matlet.2010.08.035>
23. Zhang H, Zhang G, Tang M, Zhou L, Li J, Fan X, Shi X, Qin J (2018) Synergistic effect of carbon nanotube and graphene nanoplates on the mechanical, electrical and electromagnetic interference shielding properties of polymer composites and polymer composite foams. *Chem Eng J* 353:381–393. <https://doi.org/10.1016/j.cej.2018.07.144>
24. Yue L, Pircheraghi G, Monemian SA, Manas-Zloczower I (2014) Epoxy composites with carbon nanotubes and graphene nanoplatelets—dispersion and synergy effects. *Carbon N Y* 78:268–278. <https://doi.org/10.1016/j.carbon.2014.07.003>
25. Oh JY, Jun GH, Jin S, Ryu HJ, Hong SH (2016) Enhanced electrical networks of stretchable conductors with small fraction of carbon nanotube/graphene hybrid fillers. *ACS Appl Mater Interfaces* 8:3319–3325. <https://doi.org/10.1021/acsami.5b11205>
26. Song P, Liu L, Fu S, Yu Y, Jin C, Wu Q, Zhang Y, Li Q (2013) Striking multiple synergies created by combining reduced graphene oxides and carbon nanotubes for polymer nanocomposites. *Nanotechnology* 24. <https://doi.org/10.1088/0957-4484/24/12/125704>
27. Jia LC, Yan DX, Jiang X, Pang H, Gao JF, Ren PG, Li ZM (2018) Synergistic effect of graphite and carbon nanotubes on improved electromagnetic interference shielding performance in segregated composites. *Ind Eng Chem Res* 57:11929–11938. <https://doi.org/10.1021/acs.iecr.8b03238>
28. Dey B, Ahmad MW, ALMezeni A, Sarkhel G, Bag DS, Choudhury A (2020) Enhancing electrical, mechanical, and thermal properties of polybenzimidazole by 3D carbon nanotube@graphene oxide hybrid. Elsevier Ltd. <https://doi.org/10.1016/j.coco.2019.11.012>
29. Li TT, Zhong Y, Yan M, Zhou W, Xu W, Huang SY, Sun F, Lou CW, Lin JH (2019) Synergistic effect and characterization of graphene/carbon nanotubes/polyvinyl alcohol/sodium alginate nanofibrous membranes formed using continuous needleless dynamic linear electrospinning. *Nanomaterials* 9. <https://doi.org/10.3390/nano9050714>
30. Bagotia N, Choudhary V, Sharma DK (2019) Synergistic effect of graphene/multiwalled carbon nanotube hybrid fillers on mechanical, electrical and EMI shielding properties of polycarbonate/ethylene methyl acrylate nanocomposites. Elsevier Ltd. <https://doi.org/10.1016/j.compositesb.2018.10.009>
31. Rostami A, Moosavi MI (2020) High-performance thermoplastic polyurethane nanocomposites induced by hybrid application of functionalized graphene and carbon nanotubes. *J Appl Polym Sci* 137:1–11. <https://doi.org/10.1002/app.48520>
32. Kuester S, Demarquette NR, Ferreira JC, Soares BG, Barra GMO (2017) Hybrid nanocomposites of thermoplastic elastomer and carbon nanoadditives for electromagnetic shielding. *Eur Polym J* 88:328–339. <https://doi.org/10.1016/j.eurpolymj.2017.01.023>
33. Mondal S, Khastgir D (2017) Elastomer reinforcement by graphene nanoplatelets and synergistic improvements of electrical and mechanical properties of composites by hybrid nano fillers of graphene-carbon black & graphene-MWCNT. *Compos Part A Appl Sci Manuf* 102:154–165. <https://doi.org/10.1016/j.compositesa.2017.08.003>
34. Qin Y, Qu M, Pan Y, Zhang C, Schubert DW (2020) Fabrication, characterization and modelling of triple hierarchic PET/CB/TPU composite fibres for strain sensing. *Compos Part A Appl Sci Manuf* 129:105724. <https://doi.org/10.1016/j.compositesa.2019.105724>
35. Xu H, Schubert DW (2020) Perpendicular and in-plane conductivity of poly(methyl methacrylate) composite films filled with carbon-based fillers prepared from solution casting process. *Macromol Mater Eng* 305:1–8. <https://doi.org/10.1002/mame.202000107>
36. Luo X, Qu M, Schubert DW (2020) Electrical conductivity and fiber orientation of poly (methyl methacrylate)/carbon fiber composite sheets with various thickness. *Polym Compos* 42:548–558
37. Qu M, Nilsson F, Qin Y, Yang G, Gao Q, Xu W, Liu X, Schubert DW (2020) Electrical conductivity of anisotropic PMMA composite filaments with aligned carbon fibers—predicting the influence of measurement direction. *RSC Adv* 10:4156–4165

38. Schubert DW (2018) Novel theoretical self-consistent mean-field approach to describe the conductivity of carbon fiber filled thermoplastics—PART I—theory. *Macromol Theory Simulations* 27:1700104
39. Zhao W, Chen L, Hu S, Shi Z, Gao X, Silberschmidt VV (2020) Printed hydrogel nanocomposites: fine-tuning nanostructure for anisotropic mechanical and conductive properties. *Adv Compos Hybrid Mater* 3:315–324. <https://doi.org/10.1007/s42114-020-00161-5>
40. Brown SC, Robert C, Koutsos V, Ray D (2020) Methods of modifying through-thickness electrical conductivity of CFRP for use in structural health monitoring, and its effect on mechanical properties – A review. *Compos Part A Appl Sci Manuf* 133:105885. <https://doi.org/10.1016/j.compositesa.2020.105885>
41. Cheng X, Yokozeki T, Wu L, Koyanagi J, Wang H, Sun Q (2018) The enhancement effect of carbon-based nano-fillers/polyaniline hybrids on the through-thickness electric conductivity of carbon fiber reinforced polymer. *Compos Part A Appl Sci Manuf* 105:281–290. <https://doi.org/10.1016/j.compositesa.2017.12.002>
42. Asmatulu R, Bollavaram PK, Patlolla VR, Alarifi IM, Khan WS (2020) Investigating the effects of metallic submicron and nanofilms on fiber-reinforced composites for lightning strike protection and EMI shielding. *Adv Compos Hybrid Mater* 3:66–83. <https://doi.org/10.1007/s42114-020-00135-7>
43. Huang J, Zhu Y, Jiang W, Tang Q (2015) Parallel carbon nanotube stripes in polymer thin film with tunable microstructures and anisotropic conductive properties. *Compos Part A Appl Sci Manuf* 69:240–246. <https://doi.org/10.1016/j.compositesa.2014.11.023>
44. Yong S, Chan Y, Wang M, Nam J, Suhr J (2020) Anisotropic electromagnetic interference shielding properties of polymer-based composites with magnetically-responsive aligned Fe₃O₄ decorated reduced graphene oxide. *Eur Polym J* 127:109595. <https://doi.org/10.1016/j.eurpolymj.2020.109595>
45. Shi YD, Yu HO, Li J, Tan YJ, Chen YF, Wang M, Wu H, Guo S (2018) Low magnetic field-induced alignment of nickel particles in segregated poly(L-lactide)/poly(ϵ -caprolactone)/multi-walled carbon nanotube nanocomposites: Towards remarkable and tunable conductive anisotropy. *Chem Eng J* 347:472–482. <https://doi.org/10.1016/j.cej.2018.04.147>
46. Wu S, Ladani RB, Zhang J, Bafekrpour E, Ghorbani K, Mouritz AP, Kinloch AJ, Wang CH (2015) Aligning multilayer graphene flakes with an external electric field to improve multifunctional properties of epoxy nanocomposites. *Carbon N Y* 94:607–618. <https://doi.org/10.1016/j.carbon.2015.07.026>
47. Huang Wu LTD, Brian R (2013) Dispersion optimization of exfoliated graphene nanoplatelet in polyetherimide nanocomposites: extrusion, precoating, and solid state ball milling. *Polym Compos* 37:1–14
48. Suherman H, Sulong AB, Sahari J (2013) Effect of the compression molding parameters on the in-plane and through-plane conductivity of carbon nanotubes/graphite/epoxy nanocomposites as bipolar plate material for a polymer electrolyte membrane fuel cell. *Ceram Int* 39:1277–1284. <https://doi.org/10.1016/j.ceramint.2012.07.059>
49. Legge EJ, Paton KR, Wywijas M, McMahon G, Pemberton R, Kumar N, Aranga Raju AP, Dawson CP, Strudwick AJ, Bradley JW (2020) Determining the level and location of functional groups on few-layer graphene and their effect on the mechanical properties of nanocomposites. *ACS Appl Mater Interfaces* 12:3481–13493
50. De Menezes BRC, Ferreira FV, Silva BC, Simonetti EAN, Bastos TM, Cividanes LS, Thim GP (2018) Effects of octadecylamine functionalization of carbon nanotubes on dispersion, polarity, and mechanical properties of CNT/HDPE nanocomposites. *J Mater Sci* 53:14311–14327
51. Tomova A, Gentile G, Grozdanov A, Errico ME, Paunovic P, Avella M, Dimitrov AT (2016) Functionalization and characterization of MWCNT produced by different methods. *Acta Phys Pol A* 129:405–408. <https://doi.org/10.12693/APhysPolA.129.405>
52. Luo X, Schubert DW (2021) Examining the contribution of factors affecting the electrical behavior of poly(methyl methacrylate)/graphene nanoplatelets composites. *J Appl Polym Sci* 138:1–12. <https://doi.org/10.1002/app.50694>
53. McLachlan (1990) Electrical resistivity of composites. *Phys Rev B* 46:11247–11249. <https://doi.org/10.1103/PhysRevB.46.11247>
54. Sahimi M (1994) Applications of percolation theory. CRC Press
55. Zhou W, Sasaki S, Kawasaki A (2014) Effective control of nano-defects in multiwalled carbon nanotubes by acid treatment. *Carbon N Y* 78:121–129. <https://doi.org/10.1016/j.carbon.2014.06.055>
56. Ma L-F, Bao R-Y, Dou R, Zheng S-D, Liu Z-Y, Zhang R-Y, Yang M-B, Yang W (2016) Conductive thermoplastic vulcanizates (TPVs) based on polypropylene (PP)/ethylene-propylene-diene rubber (EPDM) blend: From strain sensor to highly stretchable conductor. *Compos Sci Technol* 128:176–184
57. Kashfipour MA, Mehra N, Zhu J (2018) A review on the role of interface in mechanical, thermal, and electrical properties of polymer composites. *Adv Compos Hybrid Mater* 1:415–439. <https://doi.org/10.1007/s42114-018-0022-9>
58. Dang ZM, Shehzad K, Zha JW, Mujahid A, Hussain T, Nie J, Shi CY (2011) Complementary percolation characteristics of carbon fillers based electrically percolative thermoplastic elastomer composites. *Compos Sci Technol* 72:28–35. <https://doi.org/10.1016/j.compscitech.2011.08.020>
59. Chen L, Zhang J (2021) Designs of conductive polymer composites with exceptional reproducibility of positive temperature coefficient effect: a review. *J Appl Polym Sci* 138:1–14. <https://doi.org/10.1002/app.49677>
60. Li CQ, Zha JW, Li ZJ, Zhang DL, Wang SJ, Dang ZM (2018) Towards balanced mechanical and electrical properties of thermoplastic vulcanizates composites via unique synergistic effects of single-walled carbon nanotubes and graphene. *Compos Sci Technol* 157:134–143. <https://doi.org/10.1016/j.compscitech.2018.01.038>
61. Han S, Meng Q, Pan X, Liu T, Zhang S, Wang Y, Haridy S, Araby S (2019) Synergistic effect of graphene and carbon nanotube on lap shear strength and electrical conductivity of epoxy adhesives. *J Appl Polym Sci* 136:1–11. <https://doi.org/10.1002/app.48056>
62. Yousefi N, Sun X, Lin X, Shen X, Jia J, Zhang B, Tang B, Chan M, Kim JK (2014) Highly aligned graphene/polymer nanocomposites with excellent dielectric properties for high-performance electromagnetic interference shielding. *Adv Mater* 26:5480–5487. <https://doi.org/10.1002/adma.201305293>
63. Xia X, Hao J, Wang Y, Zhong Z, Weng GJ (2017) Theory of electrical conductivity and dielectric permittivity of highly aligned graphene-based nanocomposites. *J Phys Condens Matter* 29. <https://doi.org/10.1088/1361-648X/aa68ec>

Publisher's Note Springer Nature remains neutral with regard to jurisdictional claims in published maps and institutional affiliations.